Analytic Study of MHD Equilibria of the Belt Pinch

in "Belt-Pinch Coordinates"

G. Becker

IPP 1/140 January 1974

MAX-PLANCK-INSTITUT FÜR PLASMAPHYSIK

GARCHING BEI MÜNCHEN

MAX-PLANCK-INSTITUT FÜR PLASMAPHYSIK

GARCHING BEI MÜNCHEN

Analytic Study of MHD Equilibria of the Belt Pinch in "Belt-Pinch Coordinates"

G. Becker

IPP 1/140 January 1974

Die nachstehende Arbeit wurde im Rahmen des Vertrages zwischen dem Max-Planck-Institut für Plasmaphysik und der Europäischen Atomgemeinschaft über die Zusammenarbeit auf dem Gebiete der Plasmaphysik durchgeführt.

IPP 1/140 G. Becker

Analytic Study of MHD Equilibria of the Belt Pinch in "Belt-Pinch Coordinates"

(in English)

January 1974

ABSTRACT. MHD equilibria for belt-pinches with arbitrary half-axis ratios $\frac{a}{b}$ are studied by analytic methods. A straight pinch with sharp pressure profile, an axial surface current on a perfectly conducting plasma and a closed, perfectly conducting wall are assumed. The calculation is made in coordinate systems where plasma surface and wall are coordinate surfaces.

First an exact equilibrium for a model with a semi-infinite plasma slab between parallel walls is derived by conformal mapping ($\frac{a}{b} \to \infty$). The plasma thickness is equal to one half of the wall distance. This means that a radial compression ratio $\varkappa_b > 2$ cannot be achieved. In contrast to elliptic plasma cross sections the crossing point of the magnetic field here does not approach the plasma with increasing $\frac{a}{b}$. This result is ascribed to the almost semi-circular shape of the plasma end. Then for finite $\frac{a}{b}$ analytic solutions of the equilibrium are derived. The plasma surface and the wall are transformed to Cartesian coordinates by conformal mapping. A class of mapping functions $\zeta = \cosh^{-1}(\eta \tanh z)$ is found that yields nearly exact equilibria. η is a constant that determines $\frac{a}{b}$. The "natural" orthogonal coordinates of the belt-pinch are presented in a parametric form. The magnetic induction on the flux surfaces is calculated in these coordinates. With this method the computation time is only a few seconds. Large $\varkappa_b$- values are only obtained for surprisingly small $\frac{a}{b}$ (<1.2).

One finds $\varkappa_b = 2.2$ already at $\frac{a}{b} = 2$. $\varkappa_b$ can be slightly increased by a doublet-shaped wall. The semi-infinite slab result is the asymptotic value of the $\varkappa_b$ vs $\frac{a}{b}$ curve for $\frac{a}{b} \to \infty$. The small deviation of the results from exact solutions (for larger $\frac{a}{b}$) is reduced by applying the method of conformal mapping of nearly circular domains onto exactly circular domains. It is thus shown that a change of plasma shape influences the distribution of flux lines continuously and only by a very small amount.

1. INTRODUCTION

Non-circular cross sections of pinch plasmas are experimentally achieved by a conducting wall (flux surface) or by conductors with a prescribed current distribution. It is obvious that the plasma cross section will be almost circular if the wall is far away. Therefore, a non-circular plasma cross section with a large half-axis ratio can be produced by a conducting wall only if the distance between plasma and wall is not large compared with the plasma thickness. In our opinion the equilibria due to a conducting wall are of great practical importance, since in this case strong wall stabilization of long wavelength MHD modes can be expected. The reason is that here the instability induces large image currents in a low-inductance wall because of the small plasma-wall distance.

In connection with the belt-pinch programme at Garching this paper uses an analytic method to study non-circular MHD equilibria of arbitrary half-axis ratios $\frac{a}{b}$, where a is the large and b is the small half-axis (see Fig.1). The principal aim of the paper is to find analytic solutions for the equilibrium plasma shape that is exclusively produced by the presence of a closed wall with a self-consistent current distribution. The calculation is done in a "natural" coordinate system where all flux surfaces including the plasma surface and the wall are coordinate surfaces. It can provide a basis for a convenient stability analysis in a surface current model that includes the strong wall stabilization to be expected for this case.

Another aim of this study is to determine the maximum compression ratios that are possible in the direction of the small half-axis ($\varkappa_b$ radial compression ratio). For a given total plasma current the radial compression should be largest with a surface current distribution.

For simplicity an axially homogeneous, straight pinch is treated. The model further assumes a rectangular plasma pressure profile, axial surface currents on a perfectly conducting plasma, a vacuum field region and a closed, perfectly conducting wall. All surfaces of constant poloidal flux are surfaces of the "natural" coordinate system that is appropriate for the belt-pinch geometry. The 2- dimensional problem is solved by means of conformal mapping, i.e. by transforming all flux surfaces including the plasma surface and the wall to Cartesian coordinates.

2. EXACT ANALYTIC SOLUTION OF MHD EQUILIBRIUM OF A SEMI-INFINITE PLASMA SLAB

In this section an exact solution of the MHD equilibrium of a semi-infinite plasma slab between infinite parallel walls (see Fig.2) is analytically derived. It represents the limiting case of infinite half-axis ratio ($\frac{a}{b} \to \infty$). At the same time the analytic method of solution is demonstrated. A free boundary problem of an elliptic differential equation (Laplace's equation) has to be solved which is analogous to the so-called Helmholtz flow [1]. The mapping function and its inverse are determined by a Schwarz-Christoffel transformation [2] from the coordinate system in Fig.2 (z-plane, $z = x + iy$) onto the Cartesian coordinate

system (ζ - plane, $\zeta = \Psi + i\,\chi$) :

$$z = \frac{1}{\alpha} \ln \left[\cosh (i\,\beta\,\zeta) \right] \tag{1}$$

$$\zeta = \frac{1}{i\beta} \cosh^{-1} (e^{\alpha z}) \tag{2}$$

where $\alpha = \frac{\pi}{2d}$, $\beta = \frac{\alpha}{B_o}$, d is half the wall distance and B_o is the asymptotic magnetic induction and also the field on the equilibrium surface. The curves of constant Ψ and χ correspond to the lines of constant poloidal flux and to the lines of constant magnetic potential, respectively. By separating real and imaginary parts of Eq.(1) a parametric representation of the curves in the z-plane is obtained :

$$x = \frac{d}{\pi} \ln (\cosh^2 \beta\,\chi \,.\, \cos^2 \beta\,\Psi + \sinh^2 \beta\,\chi \,.\, \sin^2 \beta\,\Psi) \tag{3}$$

$$y = -\frac{2d}{\pi} \tan^{-1} (\tanh \beta\,\chi \,.\, \tan \beta\,\Psi) \tag{4}$$

Figure 2 shows curves with constant Ψ, i.e. flux lines (20 equidistant Ψ-values). The orthogonal curves χ = const were not drawn. The negative x-axis is the $\chi = 0$ curve. $\Psi = 0$ yields a branch cut on the positive x-axis, and $\Psi = \Psi_w = \pm \frac{\pi}{2\beta}$ the infinite walls. The dotted curve marks the exact equilibrium surface ($\Psi = \Psi_e$). At first the branch cut and the walls shall carry the axial current. Then the plasma surface is placed on $\Psi = \Psi_e$ and the surface current on the plasma replaces the current on the branch cut.

The magnetic induction is given by $B = \left| \frac{d\zeta}{dz} \right|$. From Eq.(2) it follows that

$$\frac{d\zeta}{dz} = \frac{1}{i\beta} \frac{\alpha\, e^{\alpha z}}{(e^{2\alpha z}-1)^{1/2}} = - i \frac{B_o}{(1 - e^{-2\alpha z})^{1/2}}$$

Substituting Eq.(1) yields

$$\frac{d\zeta}{dz} = - i \frac{B_o}{\tanh(i\beta\zeta)}$$

and B in curvilinear orthogonal coordinates reads

$$B = B_o \left(\frac{\sinh^2\beta\,\chi + \cos^2\beta\,\psi}{\sinh^2\beta\,\chi + \sin^2\beta\,\psi} \right)^{1/2} \tag{5}$$

It is obvious that on the equilibrium surface $\psi = \psi_e$ the magnetic induction (B_o) must not depend on χ. This is true for $\psi_e = \frac{\pi}{4\beta} = \frac{1}{2}\psi_w$. According to Eq.(4) $y = -\frac{d}{2}$ for $\chi \to \infty$ and $\psi = \psi_e$. This means that a plasma bounded by $\psi = \psi_e$ is in an exact equilibrium and has an asymptotic thickness equal to one half of the wall distance:

$$2\,b = d \tag{6}$$

The poloidal flux within the plasma is zero, since a surface current plasma is field-free in the interior. Therefore, in the vacuum field region between plasma and wall ψ has to be substituted by $\psi - \psi_e$. The magnetic induction on the negative x-axis decays very rapidly according to

$$B\,(x\,;\,y = 0) = \frac{B_o}{(e^{-2\alpha x}-1)^{1/2}} \tag{7}$$

for $e^{2\alpha|x|} \gg 1$ B decays exponentially. For the magnetic induction

or the current density j on the walls one obtains

$$\frac{B(x;y=d)}{B_o} = \frac{j(x;\ y=d)}{j_o} = (1 + e^{-2\alpha x})^{-1/2} \qquad (8)$$

The most significant results of this calculation are:

1) An exact equilibrium exists for a plasma with a very elongated shape between two parallel walls.
2) The plasma end has an almost semi-circular shape, and the crossing point of the magnetic field does not approach the plasma surface for large half-axis ratios.
3) A radial compression ratio $\varkappa_b > 2$ cannot be achieved even for a surface current distribution.

For an elliptic plasma cross section it is evident that with increasing $\frac{a}{b}$ the curvature at the plasma ends grows, and consequently B decreases more and more rapidly with the distance from the plasma. This means that the crossing point of the magnetic field (B = 0) comes too close to the plasma for large $\frac{a}{b}$. In this respect "racetrack"-like cross sections that are discussed in this paper are superior.

3. ANALYTIC SOLUTIONS OF MHD EQUILIBRIA FOR ARBITRARY HALF-AXIS RATIOS

The problem now consists in finding a free boundary solution of the Laplace equation which is analogous to the so-called Riabouchinsky flow [1]. We now look for a class of conformal mapping functions that transforms "natural" coordinates of the belt-pinch geometry for various $\frac{a}{b}$ to Cartesian coordinates. It

is solved by means of intermediary mapping by functions with well-known mapping properties. Configurations with an axial current on a branch cut like that in the z-plane of Fig.3 should from intuitive arguments have a marginal curve that separates an interior region with $B_1 > B_2$ (see Fig.1) from an exterior region with $B_1 < B_2$, and that can, in principle, be an equilibrium surface. By the way, it can be shown by the above analysis that elliptic coordinates cannot be used to describe belt-pinch equilibria in "natural" coordinates because an equilibrium surface with finite Ψ does not exist ($\Psi_e \to \infty$).

A large number of conformal mapping functions are tested by the method demonstrated in the preceding section. A successive intermediary mapping (see.Fig.3) of Cartesian coordinates ($\zeta = \Psi + i\,\chi$) onto elliptic coordinates ($z_1 = x_1 + i\,y_1$) by $z_1 = \cosh \zeta$ and then onto "belt-pinch coordinates" ($z = x + i\,y$) by $z = \tanh^{-1}\left(\frac{1}{\eta} z_1\right)$, with $\eta = \coth c$, yields nearly exact equilibria. The parameter c denotes half of the length of a branch cut in the z-plane and determines the various $\frac{a}{b}$ values of the equilibrium solutions (see Fig.4). By substitution one obtains the following class of mapping functions (constant factors in front have been set equal to 1) and its inverse:

$$z = \tanh^{-1}\left(\frac{1}{\eta} \cosh \zeta\right) \tag{9}$$

$$\zeta = \cosh^{-1}\left(\eta \tanh z\right) \tag{10}$$

Again the Ψ = const curves correspond to the lines of

constant poloidal flux. The coordinate lines in the z-plane are calculated by separating real and imaginary parts of Eq.(9). The following equations represent natural orthogonal coordinates of the belt-pinch in a parametric form:

$$x = \frac{1}{4} \ell n \left\{ \frac{(\eta^2 - x_1^2 - y_1^2)^2 + (2\eta y_1)^2}{[(\eta - x_1)^2 + y_1^2]^2} \right\} \tag{11}$$

$$y = \frac{1}{2} \tan^{-1} \left(\frac{2\eta y_1}{\eta^2 - x_1^2 - y_1^2} \right) \tag{12}$$

where $x_1 = \cosh \Psi \cdot \cos \chi$ and $y_1 = \sinh \Psi \cdot \sin \chi$ are derived from $z_1 = \cosh \zeta = x_1 + i\, y_1$. In Fig.5 one half of the curves of constant Ψ, i.e. flux lines, are shown for various $\frac{a}{b}$. The flux lines are plotted in steps of 0.1 Ψ_e. The orthogonal curves were not drawn. For $\Psi = 0$ the branch cut $-c \leq x \leq c$ and for $\Psi < 0$ the other flux surfaces are obtained. The dotted or dashed curves ($\Psi = \Psi_e$) mark the equilibrium solutions. It is obvious from these plots that $\frac{a}{b}$ (for $\Psi = \Psi_e$) grows when c is increased. Differentiating Eq.(10) and substituting Eq.(9) yields

$$\frac{d\zeta}{dz} = \eta \, \frac{1 - (\frac{1}{\eta} \cosh \zeta)^2}{\sinh \zeta}$$

In "natural" coordinates one obtains

$$B^2 \sim \frac{1}{\sinh^2 \psi + \sin^2 \chi} \left[\frac{1}{\eta^2} (\sinh^2 \psi + \sin^2 \chi)^2 \right.$$

$$\left. - 2(1 - \frac{1}{\eta^2}) \, (\sinh^2 \psi \cdot \cos^2 \chi - \cosh^2 \psi \cdot \sin^2 \chi) + (\eta - \frac{1}{\eta})^2 \right] \tag{13}$$

The problem is now to determine for each half-axis ratio the Ψ-value that yields the smallest χ-variation of B. It is solved analytically and numerically by very short jobs with computing times of only a few seconds. The current on the branch cut can now be replaced by a surface current on a plasma which is bounded by $\Psi = \Psi_e$. The wall as the other boundary of the vacuum field region can be placed on any flux surface ($\Psi_{crit} \leq \Psi < \Psi_e$). Ψ_e denotes the equilibrium solution and is the marginal curve which separates the $B_1 > B_2$ region from the $B_1 < B_2$ region that were mentioned above. Ψ_{crit} describes the outermost flux surface that exists in the first plane of the Riemann surface. By calculating B_1 and B_2 from Eq.(13) and by setting $B_1 = B_2$ one obtains for $\Psi > \Psi_{crit}$

$$\Psi_e = - \frac{1}{4} \ell n \, (4 \, \eta^2 - 3) \tag{14}$$

A detailed numerical study has shown that Ψ_e indeed describes a flux surface that differs only very little from the flux surface with the smallest χ - variation of B. The outermost flux surface $\Psi = \Psi_{crit}$ is derived from the condition $x \to \infty$ for $y = 0$:

$$\Psi_{crit} = - \ell n \, (\eta + \sqrt{\eta^2 - 1}) \tag{15}$$

The maximum radial compression ratio $\varkappa_b$ is obtained if the wall is placed on the outermost flux surface $\Psi = \Psi_{crit}$. $\varkappa_b$ is determined by calculating the y-value that belongs to $\Psi = \Psi_{crit}$ and $x = 0$

$$y_{crit} = -\frac{1}{2}\tan^{-1}\left(2\eta\sqrt{\eta^2-1}\right) \qquad (16)$$

and dividing it by b.

In Fig.5 the positions of y_{crit} have been marked. The c-dependence of $\frac{a}{b}$ in Fig.4 was derived analytically by inserting Eq. (14) into

$$\frac{x(\Psi=\Psi_e;\ \chi=0)}{y(\Psi=\Psi_e;\ \chi=\frac{\pi}{2})} = \frac{a}{b}\,.$$

Thus one obtains the correct c-value for the numerical calculations that corresponds to a desired half-axis ratio.

In Fig. 6 the maximum radial compression ratio $\varkappa_b$ is plotted versus $\frac{a}{b}$. One sees that large $\varkappa_b$-values are only obtained for surprisingly small $\frac{a}{b}$ (< 1.2) even with a surface current distribution. The dashed line is an extrapolation of the $\varkappa_b$-curve for $\frac{a}{b} \leq 3$. For this $\frac{a}{b}$ -range the walls on $\Psi = \Psi_{crit}$ are still nearly parallel lines. Indeed the dashed line agrees very well with the asymptotic value $\varkappa_b = 2$, that was derived above for the limiting case $\frac{a}{b} \to \infty$ and for parallel infinite walls. It is surprising, however, that already at $\frac{a}{b} = 2$ the maximum radial compression ratio is only 2.2. The growth of $\varkappa_b$ for $\frac{a}{b} > 3$ is ascribed to an increase of the doublet-shaped deformation of the wall.

In practical situations of an experiment the ratio of the coil cross section area to the plasma cross section area $\varkappa_{ab}$ is known and the question is what half-axis ratio will

ideally be reached by the plasma after contraction. Therefore in Fig.7 $\varkappa_{ab}$ is plotted versus $\frac{a}{b}$ for a given coil height to width ratio of 5.5, which holds for the Belt-Pinch II experiment. The $\varkappa_{ab}$ values have been determined from the plots of flux surfaces after placing the wall on the correct flux surface. Obviously for large $\varkappa_{ab}$ the plasma contracts to a cylinder with nearly circular cross section. Even for $\varkappa_{ab} \approx 15$ a half-axis ratio of only 2 is obtained.

A comparison of the $\Psi = \Psi_e$ curves in Fig.5 with ellipses of the same ratio $\frac{a}{b}$ shows that the plasma shape becomes more and more "racetrack"-like (semi-circles at the ends) with increasing $\frac{a}{b}$. This is in agreement with the results of section 2 and also with experimental findings. Compared with elliptic cross sections these configurations are advantageous because the separatrix does not approach the plasma with increasing $\frac{a}{b}$ (compare section 2). The reason is that for the "racetrack"-like shape the curvature radius at the ends is about equal to the small half-axis b and is therefore independent on $\frac{a}{b}$ for a fixed b-value.

The poloidal flux between plasma and wall is given by

$$|\Psi_{crit}| - |\Psi_e| = L\, I_p \qquad (17)$$

where L is the inductance of the system and I_p is the total current on the plasma surface. From Eq. (17) the $\frac{a}{b}$-dependence of the inductance is determined by assuming a fixed plasma current. The result is shown in Fig.8. Here L_o is the induc-

tance for $\frac{a}{b} = 4$, since all fluxes have been normalized to the flux for $\frac{a}{b} = 4$. It is seen that L decreases only slightly for half-axis ratios larger than 2.

In the method used an exact shape of the wall is not prescribed. Rather a mapping function is determined first that yields a desired equilibrium shape of the plasma and then the shape of the wall on one of the flux surfaces is calculated. This procedure is the opposite of that used in a numerical treatment of the problem [3], where the shape of the wall (rectangular box) is prescribed. Moreover, the model assumes a volume current distribution. The tendency towards a larger radial compression ratio with a current distribution, which is more peaked at the plasma surface, was found [3], but the surface current case could not be treated.

It can be shown that the function in square brackets in Eq.(13) may be written as

$$\frac{1}{\eta^2}\sin^4\chi + 2\left[\left(2 - \frac{1}{\eta^2}\right)\sinh^2\Psi + 1 - \frac{1}{\eta^2}\right]\sin^2\chi$$

$$+ \left[\frac{1}{\eta^2}\sinh^2\Psi - 2\left(1 - \frac{1}{\eta^2}\right)\right]\sinh^2\Psi + \left(\eta - \frac{1}{\eta}\right)^2$$

On a special flux surface ($\Psi = \Psi_o$) this function is proportional to the denominator of Eq.(13) if the $\sin^4\chi$ - term is neglected. This means that B does not depend on χ for $\Psi = \Psi_o$. Therefore the term $\tanh^2 c \cdot \sin^4\chi$ describes the deviation from the exact equilibrium surface. Obviously, this deviation grows if c and consequently $\frac{a}{b}$ is increased.

The maximum error of $B(\chi)$ on the equilibrium surface $\Psi = \Psi_e$ is defined as

$$\delta = \frac{B_{max} - B_{min}}{B_{max} + B_{min}} \tag{18}$$

A detailed numerical calculation of the χ-variation of B for the half-axis ratios of Fig.5 yields the results in Table I. As one would expect the large curvature regions of $\Psi = \Psi_e$ exhibit much steeper gradients of B perpendicular to the surface $\Psi = \Psi_e$, than those with small curvature.

TABLE I.

MAXIMUM ERRORS δ FOR THE $\frac{a}{b}$ - VALUES OF FIG. 5

$\frac{a}{b}$	1.2	1.6	2.0	3.0	4.0	6.0
δ	2×10^{-5}	8.8×10^{-4}	3.76×10^{-3}	1.87×10^{-2}	3.88×10^{-2}	7.85×10^{-2}

These numerical results agree well with the above calculation. The maximum error grows if $\frac{a}{b}$ is increased.

The deviation from exact solutions has been reduced by applying the method of conformal mapping of nearly circular domains onto exactly circular domains [4,5]. This procedure can also be regarded as a further generalization of the class of mapping functions in Eqs.(9) and (10). Instead of directly

mapping Cartesian coordinates onto elliptic coordinates (see Fig. 3), first an intermediary mapping onto polar coordinates (w-plane) is performed, where the flux surfaces are circles in the interior of the unit circle ($\Psi < 0$). The exact solution deviates very little from the flux surface and is therefore a nearly circular curve. Then the method of conformal mapping of a nearly circular domain (w_1-plane) onto an exactly circular domain (w-plane) is applied. It is described in Appendix A. Appropriately choosing the Fourier coefficients that determine the deviation from the unit circle yields a more precise equilibrium solution in all regions of the plasma surface (for all χ). A set of Fourier coefficients for this analysis can be determined by Fourier analyzing the known χ-variation of B on $\Psi = \Psi_e$. For the case $\frac{a}{b} = 4$, for example, the δ-value has been continuously reduced from 3.88% to 2% by optimizing only three coefficients ($g = -c = 0.006$ and $d = -0.008$, see Appendix A, Eq.(A5)). It has been shown that the distribution of flux lines is changed only very little and continuously when the shape of the plasma surface approaches the exact equilibrium. The accuracy of the flux line plots in Fig.5 is sufficient for experimental purposes. It is found for a fixed position of the vertex points that for all other x the $|y|$-value is slightly increased.

In Appendix B the vacuum magnetic field energy W_m is varied. It is shown by a simple model calculation for large $\frac{a}{b}$ that W_m has a minimum at a plasma thickness equal to one half of the wall distance (compare Eq.(6)).

4. SUMMARY AND CONCLUSIONS

MHD equilibria for belt-pinches with arbitrary half-axis ratios $\frac{a}{b}$ have been studied by analytic methods. A straight pinch with sharp pressure profile, axial surface currents on a perfectly conducting plasma and a vacuum field between the plasma and a closed, perfectly conducting wall are assumed. The calculation has been carried out in a "natural" coordinate system where plasma surface and wall are coordinate surfaces.

First an exact equilibrium for a simple model with a semi-infinite plasma slab between parallel and infinite walls has been derived by means of conformal mapping ($\frac{a}{b} \to \infty$). It is found at a plasma thickness equal to one half of the wall distance. This means that a radial compression ratio $\varkappa_b > 2$ cannot be achieved even for a surface current distribution that, for a given total plasma current , yields the largest compression.

Then for finite $\frac{a}{b}$ analytic solutions for the equilibrium plasma shape have been derived which can provide a basis for a stability analysis including strong wall stabilization effects. The plasma surface and the wall are transformed to Cartesian coordinates by conformal mapping. A class of mapping functions $\zeta = \cosh^{-1} (\eta \cdot \tanh z)$ has been found that yields nearly exact equilibria. η is a constant that determines the various $\frac{a}{b}$. The "natural" orthogonal coordinates of the belt-pinch have been given in a parametric form. The magnetic induction on the flux surfaces has been calculated in these coordinates. In contrast to

numerical investigations of the problem the computing time with the method developed in this paper is negligible (a few seconds). Compared with elliptic cross sections these "race-track"-like configurations are advantageous because the separatrix does not approach the plasma with increasing $\frac{a}{b}$. Large $\varkappa_b$ - values are only obtained for surprisingly small $\frac{a}{b}$ (< 1.2) even with the surface current distribution. Already at $\frac{a}{b} = 2$ $\varkappa_b$ does not exceed 2.2. The radial compression ratio can be increased slightly by a doublet-shaped wall. The semi-infinite slab result ($\frac{a}{b} \to \infty$) is indeed the asymptotic value of the extrapolated $\varkappa_b$ vs $\frac{a}{b}$ curve.

The small deviation of the results from exact solutions (for larger $\frac{a}{b}$) has been reduced by applying the method of conformally mapping nearly circular domains onto exactly circular domains. It has been shown that the distribution of flux lines is changed only very little and continuously when the shape of the plasma surface approaches the exact equilibrium.

ACKNOWLEDGEMENTS

The author wishes to thank R.Wunderlich for performing the computations during a period of several months with remarkable care and Dr. H.Wobig for fruitful discussions.

APPENDIX A: CONFORMAL MAPPING OF A NEARLY CIRCULAR DOMAIN

A nearly circular curve (see Fig.A.1) reads in polar coordinates

$$r = 1 + \epsilon\, p\,(\chi) \qquad \text{(A 1)}$$

where ϵ is a small positive parameter and $\epsilon\, p\,(\chi)$ describes the deviation from a unit circle. If the function $p\,(\chi)$ is expanded into a Fourier series

$$p\,(\chi) = a_o + \sum_{n=1}^{m} (a_n \cos n\chi + b_n \sin n\chi) \qquad \text{(A 2)}$$

the associated function that conformally maps the nearly circular domain in the w_1-plane onto the interior of the unit circle in the w-plane (see Fig. A.1) reads

$$w = w_1 + \epsilon\, w_1 \left[a_o + \sum_{n=1}^{m} (a_n - i\, b_n)\, w_1^{n}\right] \qquad \text{(A 3)}$$

Its inverse is

$$w_1 = w - \epsilon\, w \left[a_o + \sum_{n=1}^{m} (a_n - i\, b_n)\, w^{n}\right] \qquad \text{(A 4)}$$

Owing to the symmetry of the problem an ansatz

$$p(\chi) = a_o + a_4 \cos 4\chi + b_4 \sin 4\chi \qquad \text{(A 5)}$$

is made. With the abbreviations $\epsilon\, a_o = g$, $\epsilon\, a_4 = c$ and $-\epsilon\, b_4 = d$ one then obtains the following generalization of the class of mapping functions given in Eqs.(9) and (10):

$$z = \tanh^{-1}\left(\frac{1}{\eta} z_1\right) \qquad \text{(A 6)}$$

with $z_1 = \frac{1}{2}\left(e^{\Psi_e} w_1 + \frac{1}{e^{\Psi_e} w_1}\right)$ and $w_1 = w\left\{1 - [g + (c + id)w^4]\right\}$.

The inverse function reads

$$\zeta = \ln\left\{w_1 + w_1 [g + (c + id) w_1^4]\right\} \qquad \text{(A 7)}$$

with $w_1 = e^{-\Psi_e}\left(z_1 + \sqrt{z_1^2 - 1}\right)$ and $z_1 = \eta \tanh z$.

Using these generalized conformal mapping functions coordinates and fields have been calculated as in section 3. With $g = c = d = 0$, the results of section 3 have been reproduced.

APPENDIX B: MINIMUM OF VACUUM FIELD ENERGY FOR LARGE HALF-AXIS RATIO

By a rough model calculation it is shown for large $\frac{a}{b}$ that the vacuum magnetic field energy W_m has a minimum at a plasma thickness equal to one half of the wall distance (compare Eq.(6)). This result is obtained with a fixed total current on the plasma surface I_p and a fixed, but within certain limits arbitrary, plasma cross sectional area F such as is met in realistic experimental situations. The geometry of the model is shown in Fig. B.1. The vacuum magnetic field energy per unit length of the axial direction reads

$$W_m = \frac{1}{2} L I_p^2 = \frac{1}{2} \psi^2 \frac{1}{L} \qquad \text{(B 1)}$$

where L is the inductance of the system and ψ is the poloidal flux between plasma and wall. The flux $\psi = L I_p$ is a constant since plasma and wall are perfect conductors. A variation of the plasma shape causes a variation of L and W_m such that a maximum of L corresponds to a minimum of W_m. For large $\frac{a}{b}$ or, to be more precise, for $s \ll 2\ell$ the inductance per unit length of the system can be approximated by the inductance of two parallel plate transmission lines with plate distance s in parallel

$$L = \frac{1}{2} \mu_o \frac{s}{2\ell} \qquad \text{(B 2)}$$

For $s \ll 2\ell$ the magnetic field energy at the top and bottom may be neglected without introducing a significant error. Indeed it has been shown in section 2 that the magnetic induction decreases very rapidly with the distance from the plasma ends.

Substituting $s = d - h$ and $F \approx 4 \ell h$ in Eq.(B 2) gives

$$L = \frac{\mu_o}{F} (d - h)\, h \qquad \text{(B 3)}$$

Differentiating with respect to h at a fixed F yields

$$\frac{dL}{dh} = \frac{\mu_o}{F} (d - 2h) \qquad \text{(B 4)}$$

From $\frac{dL}{dh} = 0$ and $\frac{d^2L}{dh^2} < 0$ it follows that

$$2h = d \qquad \text{(B 5)}$$

is the position of maximum L and minimum W_m.

Note that Eq.(B 5) results from Eq. (B 4) for fixed, but within certain limits arbitrary, F - values.

REFERENCES

[1] GARABEDIAN,P.R., Partial Differential Equations, John Wiley, New York (1964) 538.

[2] MORSE,P.M., FESHBACH,H., Methods of Theoretical Physics, Pt.II, McGraw-Hill, New York (1953) 1247.

[3] v.HAGENOW,K., LACKNER,K., Proc. 3rd Int.Symp. on Toroidal Plasma Confinement, Garching 1973, F 7.

[4] NEHARI,Z., Conformal Mapping, McGraw-Hill, New York (1952) 263.

[5] BETZ,A., Konforme Abbildung, Springer, Berlin (1964) 297.

FIGURE CAPTIONS

Fig. 1 Definition of half-axes a and b.

Fig. 2 Flux lines of semi-infinite plasma slab between parallel walls. The dotted curve is the exact equilibrium and plasma surface.

Fig. 3 Conformal mapping of Cartesian coordinates onto "belt-pinch coordinates".

Fig. 4 Half-axis ratio $\frac{a}{b}$ versus branch cut parameter c.

Fig. 5 Upper half plot of flux lines for various $\frac{a}{b}$. The dotted or dashed curves are the equilibrium $\Psi = \Psi_e$.
(a) $\frac{a}{b} = 1.2$, (b) $\frac{a}{b} = 1.6$, (c) $\frac{a}{b} = 2.0$, (d) $\frac{a}{b} = 3.0$,
(e) $\frac{a}{b} = 4.0$, (f) $\frac{a}{b} = 6.0$

Fig. 6 Maximum radial compression ratio $\varkappa_b$ versus $\frac{a}{b}$.

Fig. 7 Ratio of coil cross section area to plasma cross section area $\varkappa_{ab}$ versus $\frac{a}{b}$ for a coil height to width ratio of 5.5.

Fig. 8 Inductance L versus $\frac{a}{b}$ normalized to L_o, the inductance for $\frac{a}{b} = 4$.

Fig.A1 Conformal mapping of a nearly circular domain.

Fig.B1 Variation of magnetic field energy W_m. Cross section of plasma and wall.

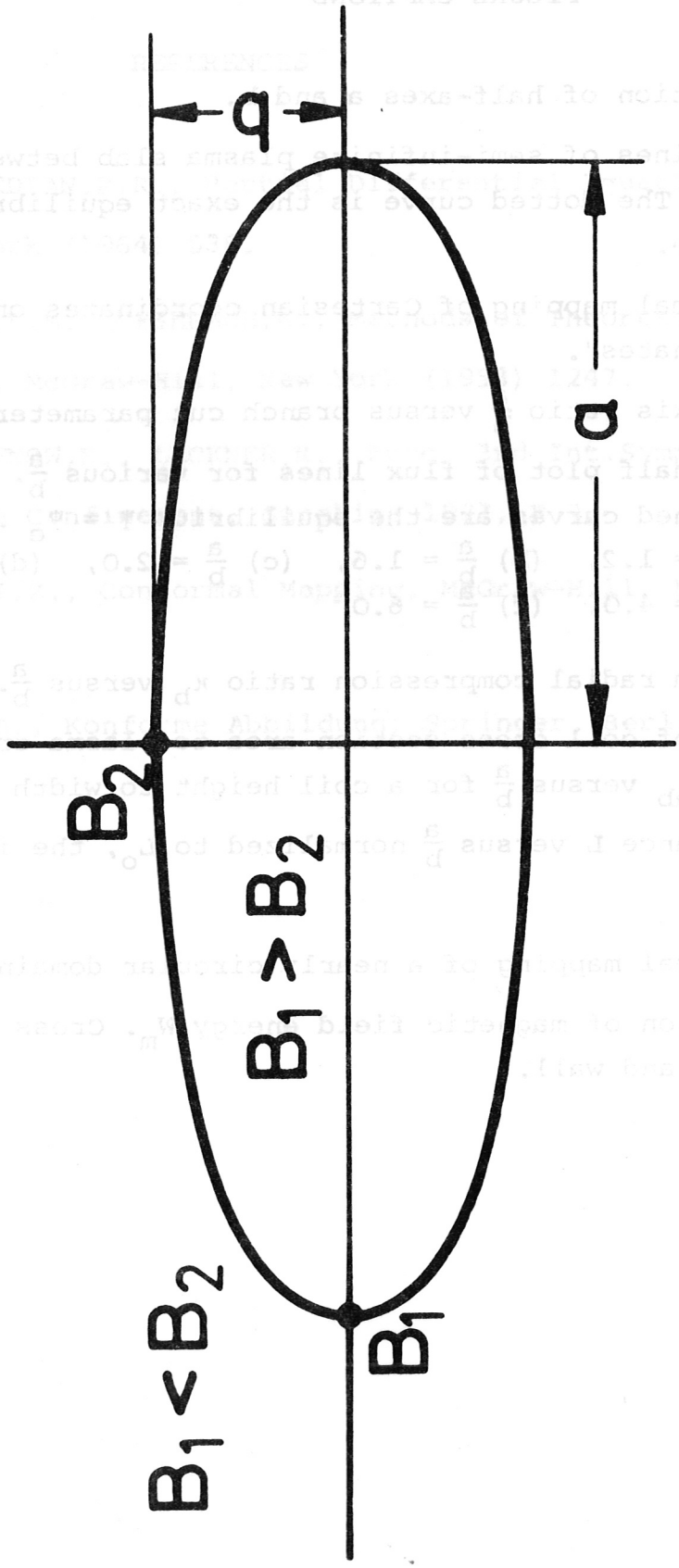

Fig. 1

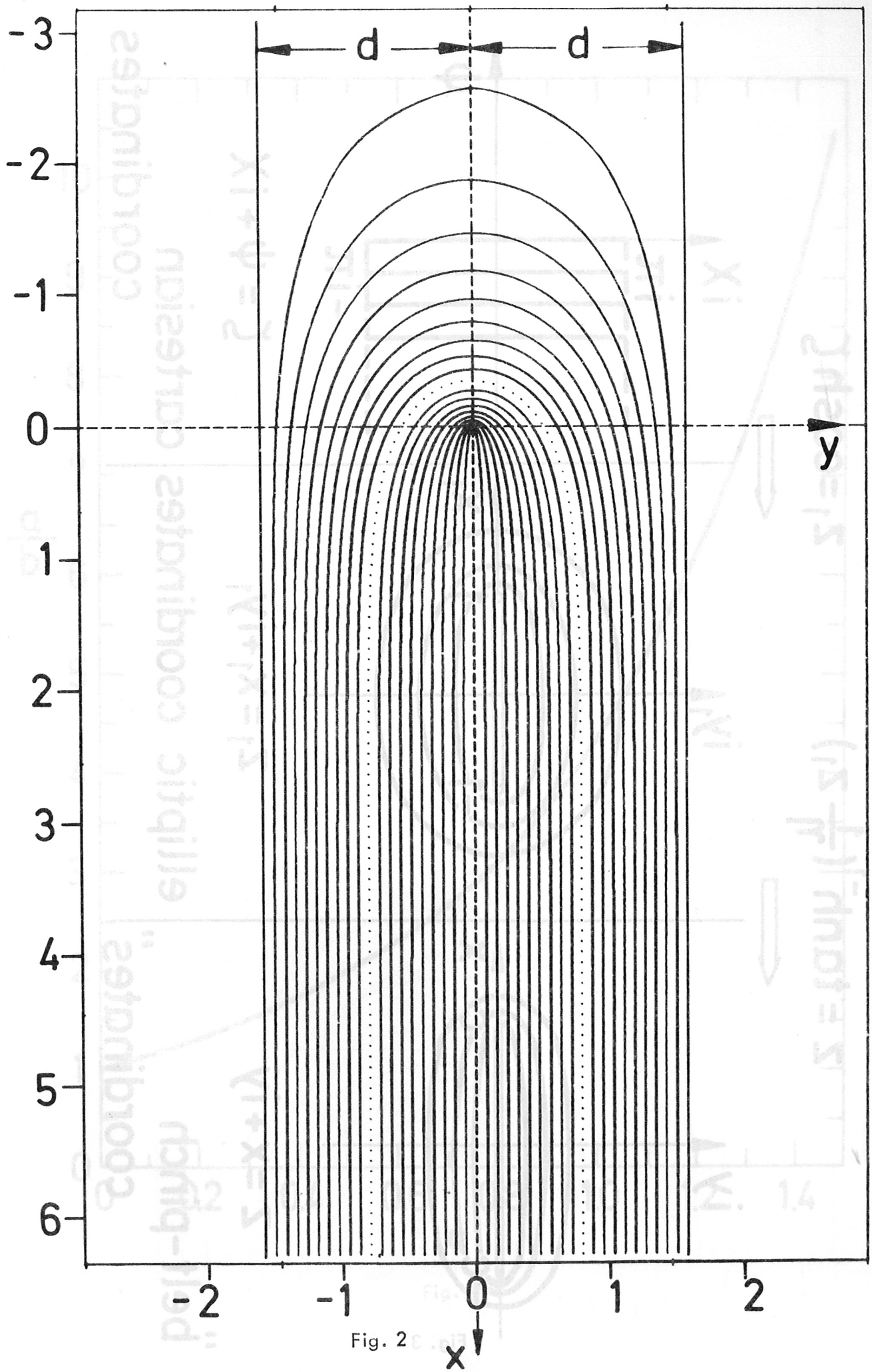

Fig. 2

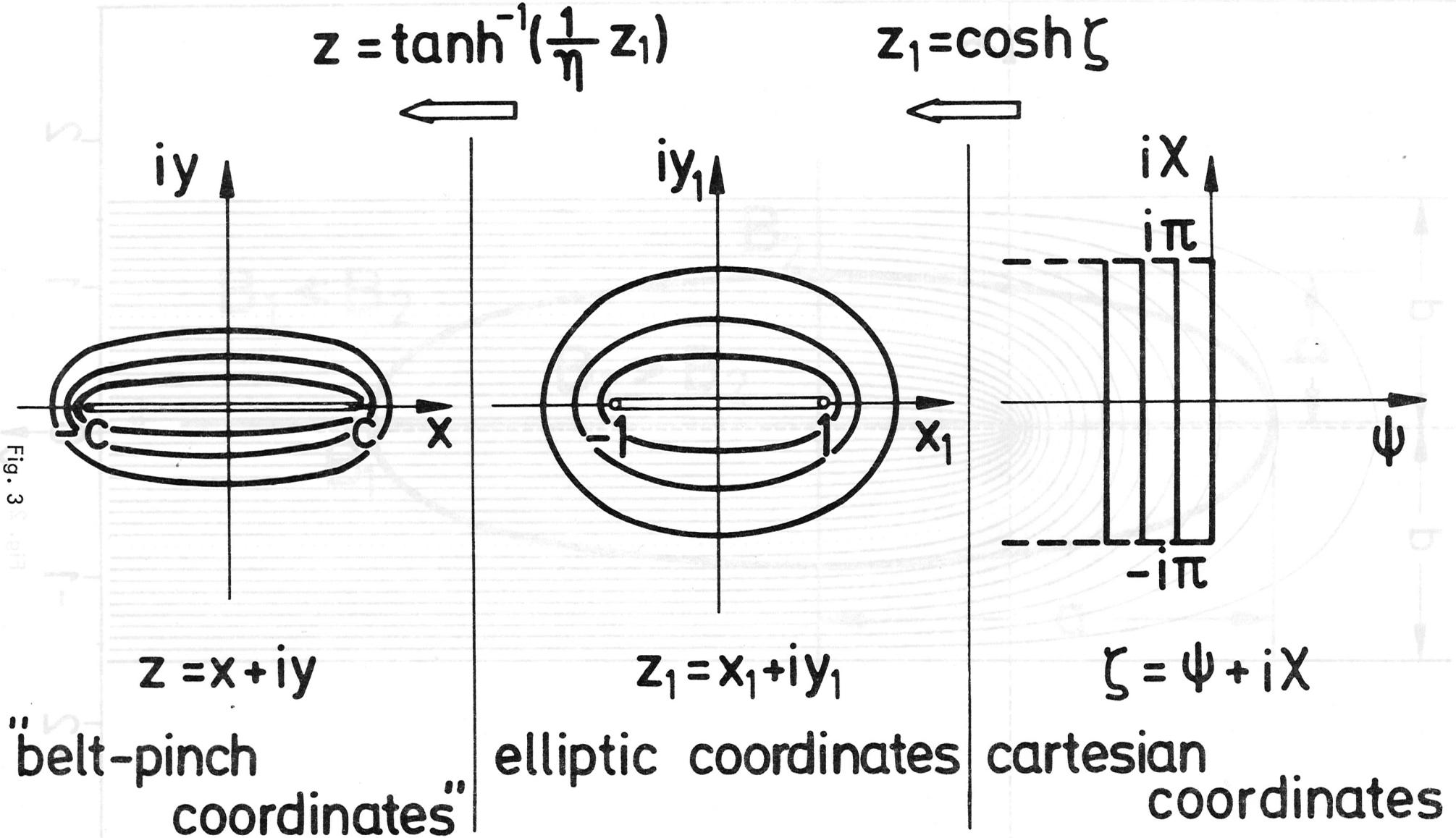
$z = \tanh^{-1}(\frac{1}{\eta} z_1)$
$z_1 = \cosh \zeta$
iy
x
C
C
iy_1
x_1
-1
1
iX
iπ
$-i\pi$
Ψ
$z = x + iy$
$z_1 = x_1 + iy_1$
$\zeta = \Psi + iX$
"belt-pinch coordinates"
elliptic coordinates
cartesian coordinates

Fig. 3

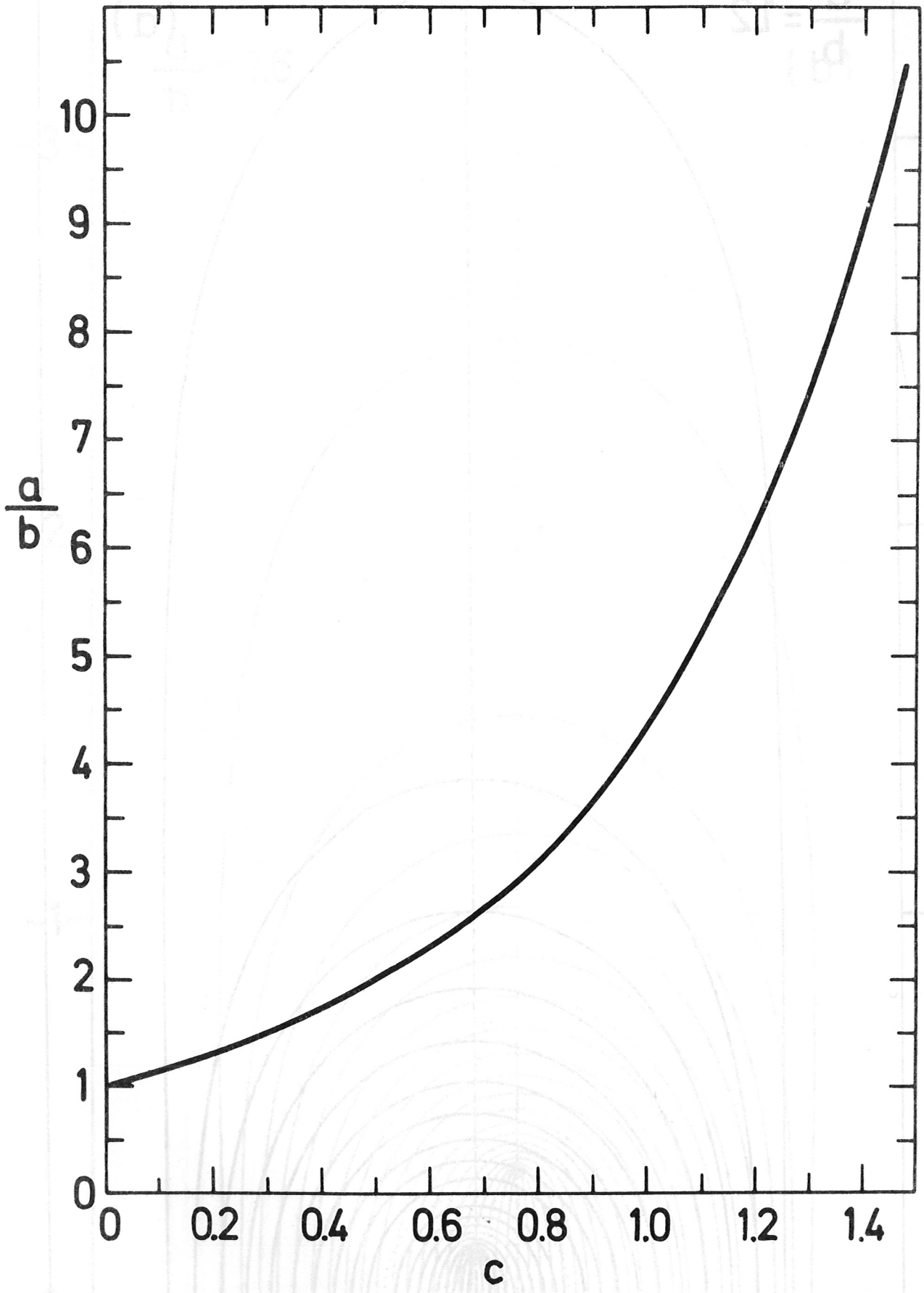

Fig. 4

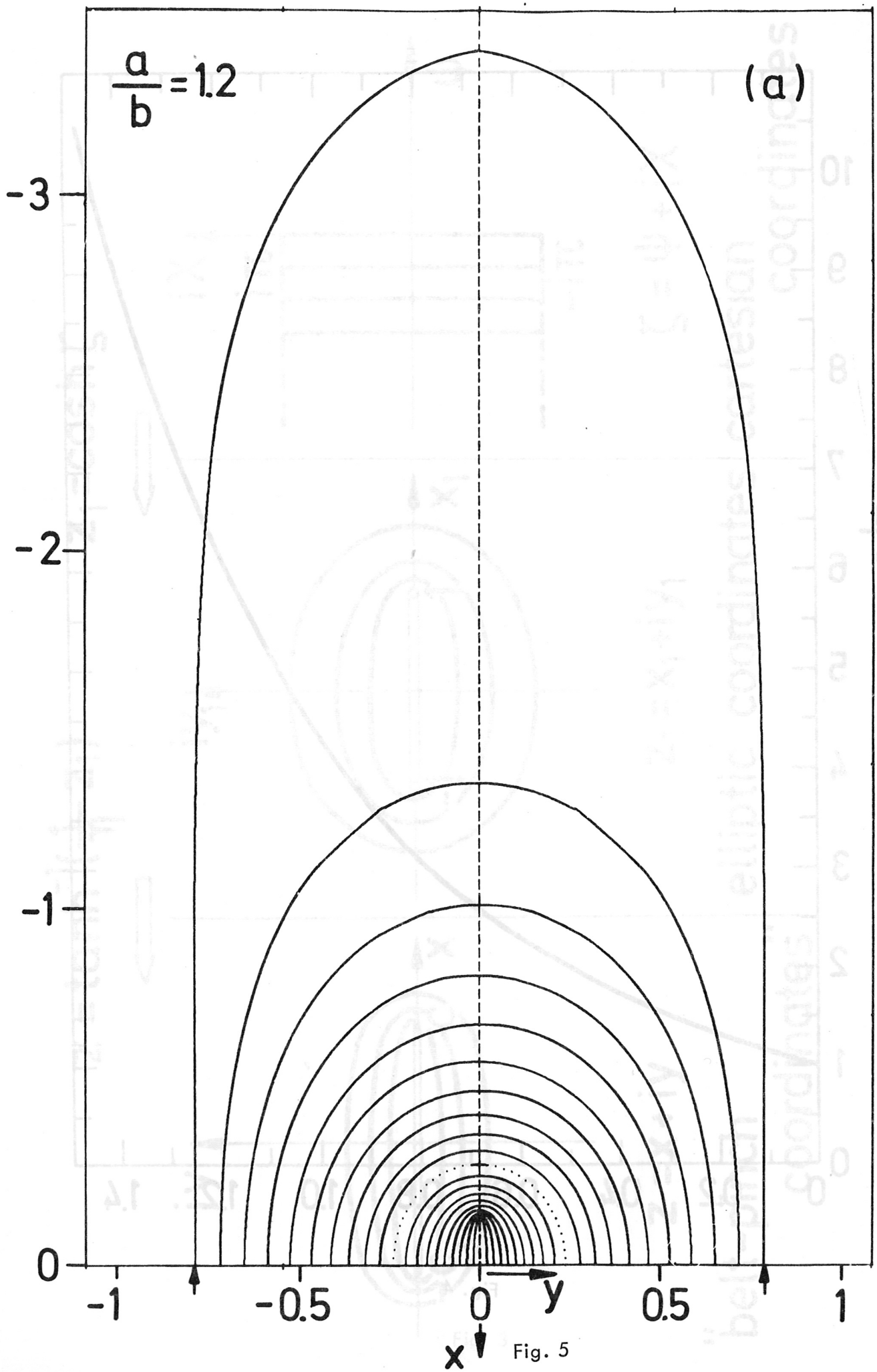

Fig. 5

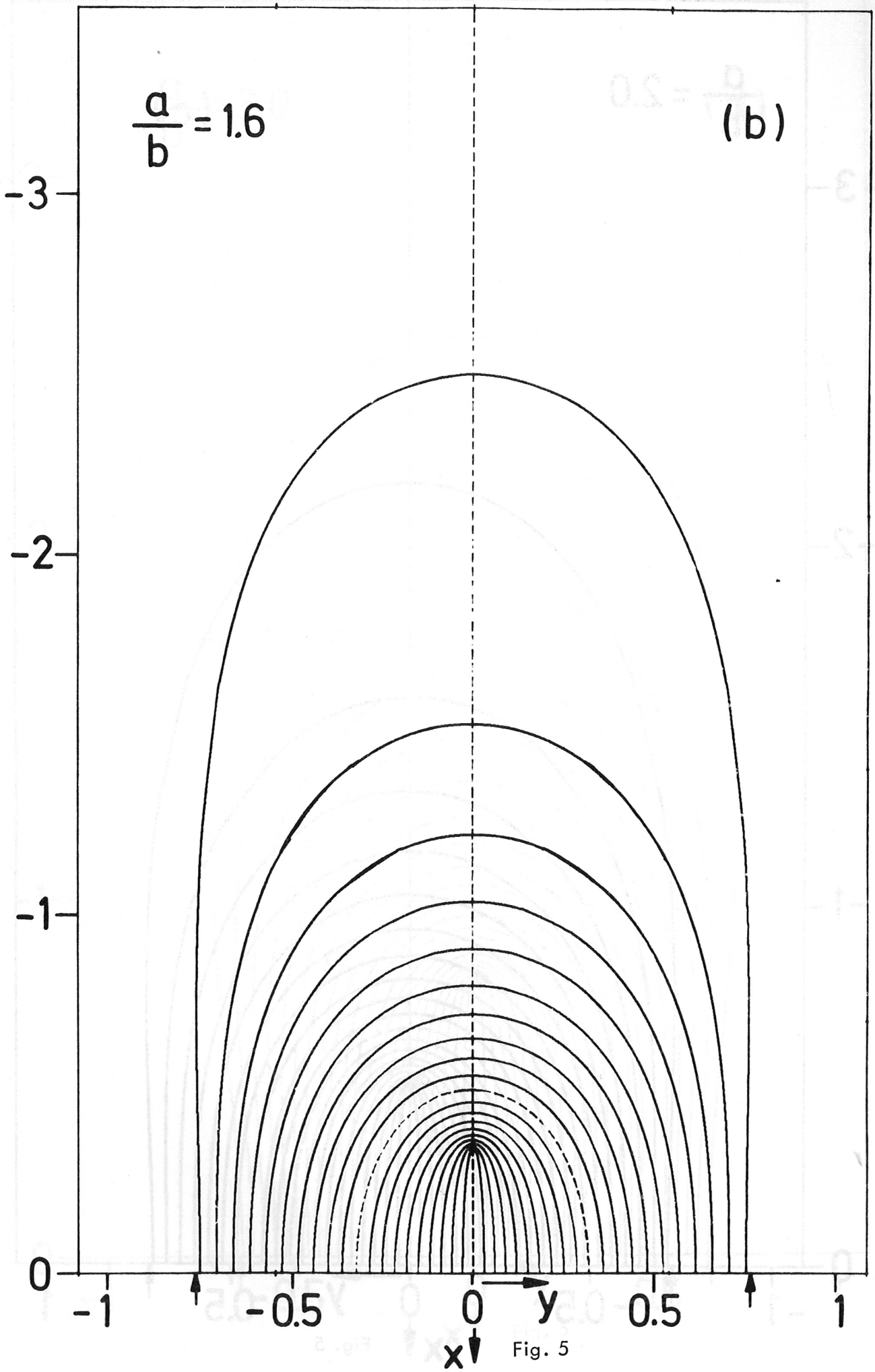

Fig. 5

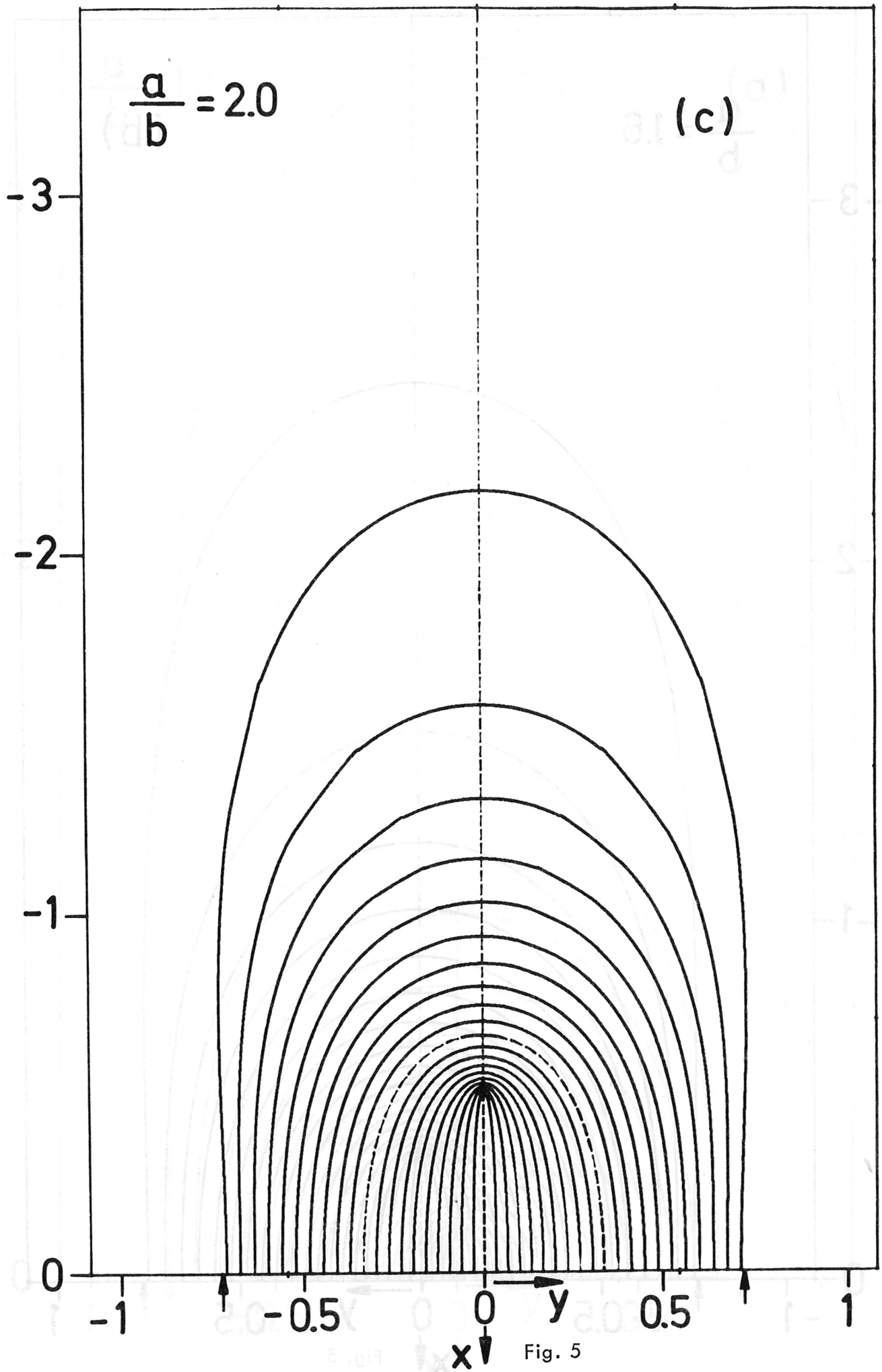

Fig. 5

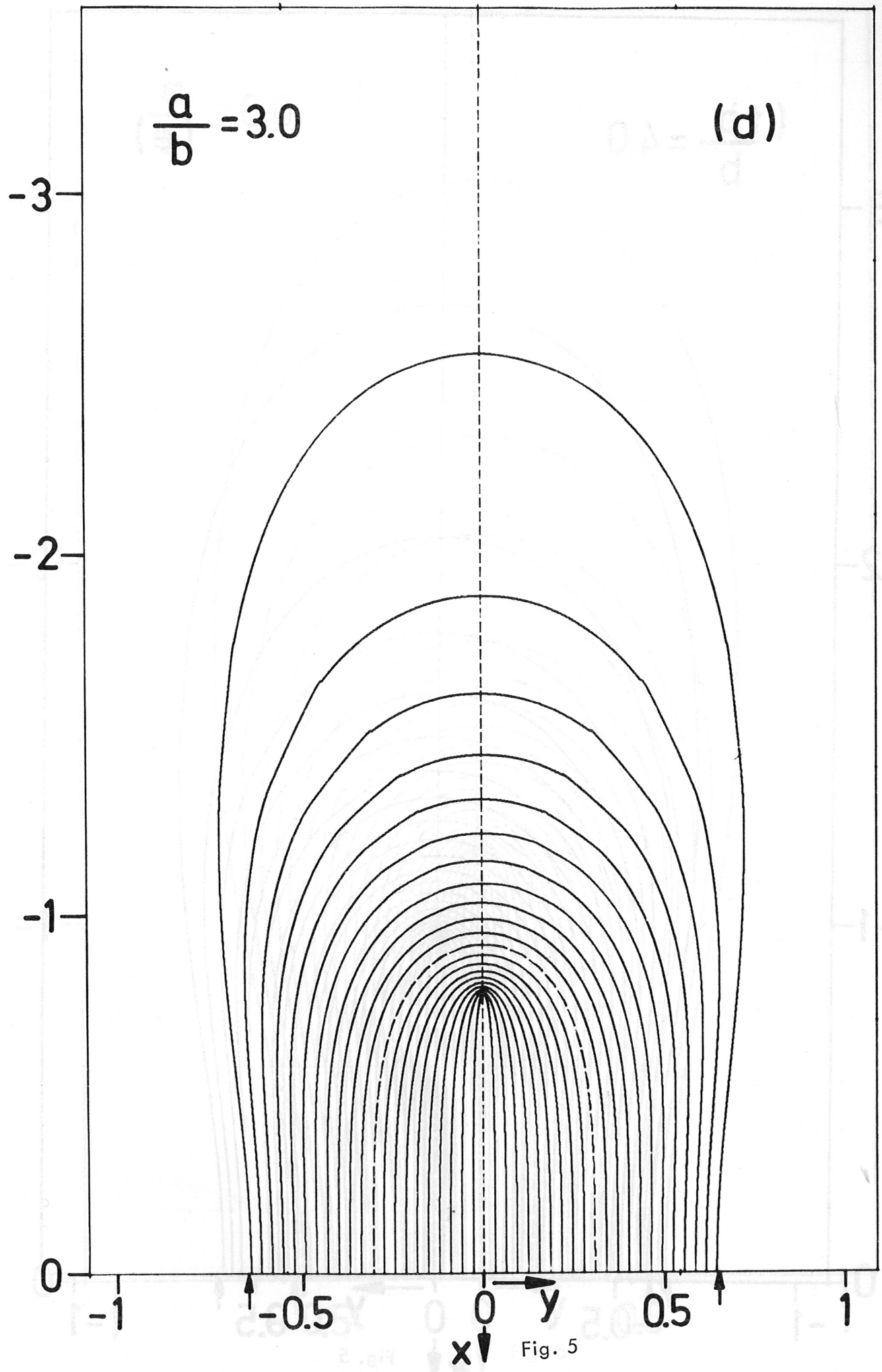

Fig. 5

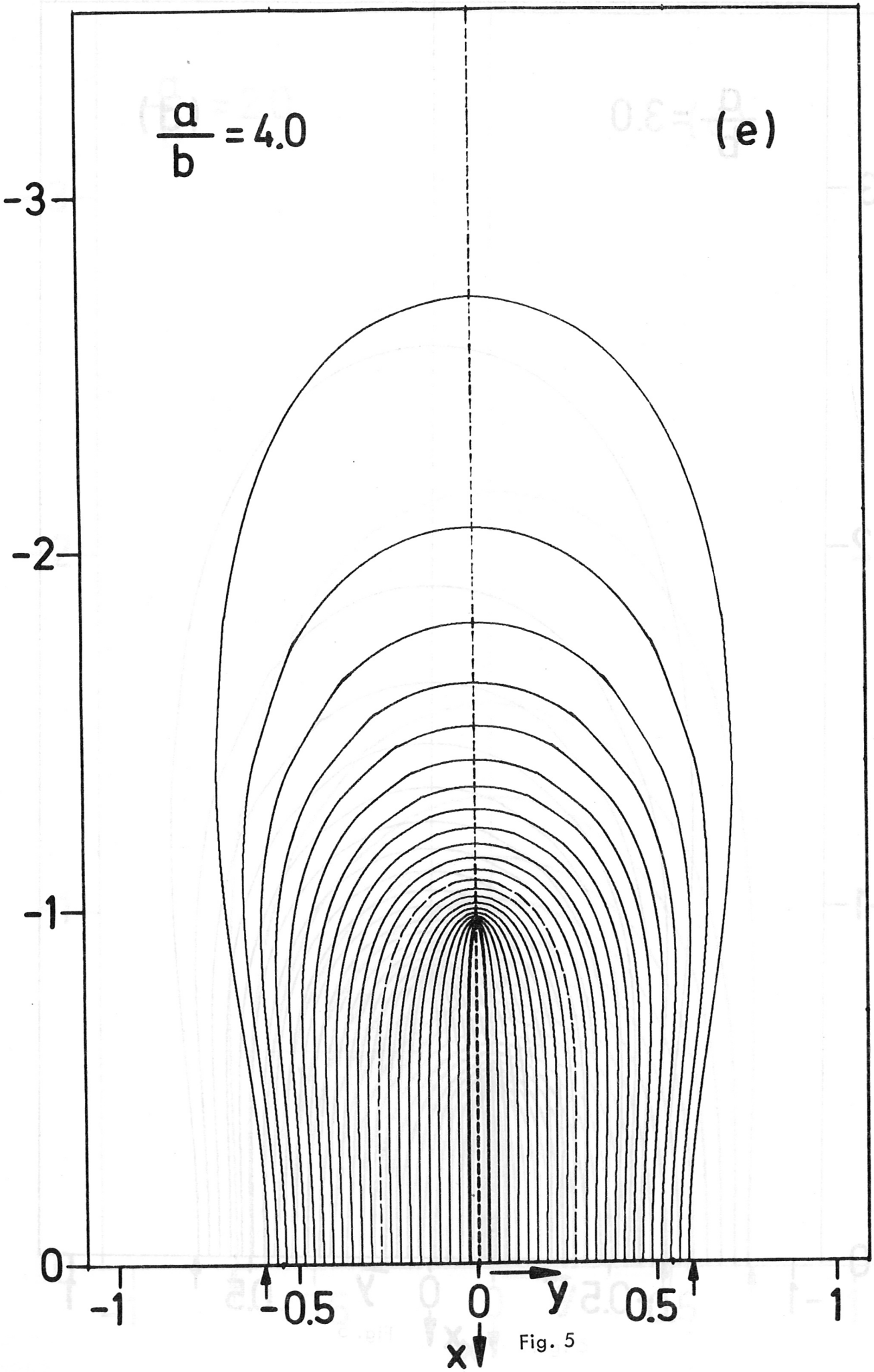

Fig. 5

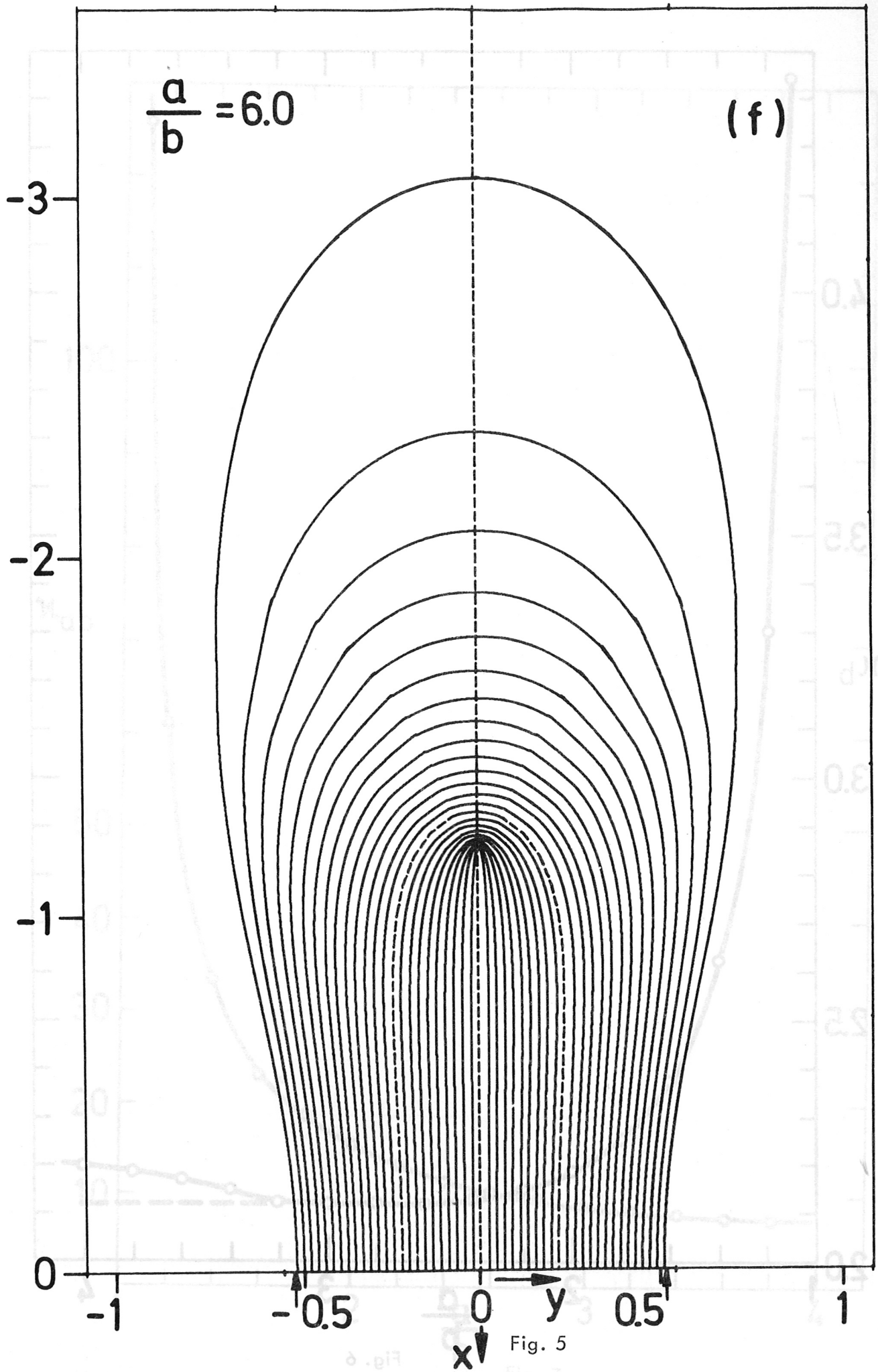

Fig. 5

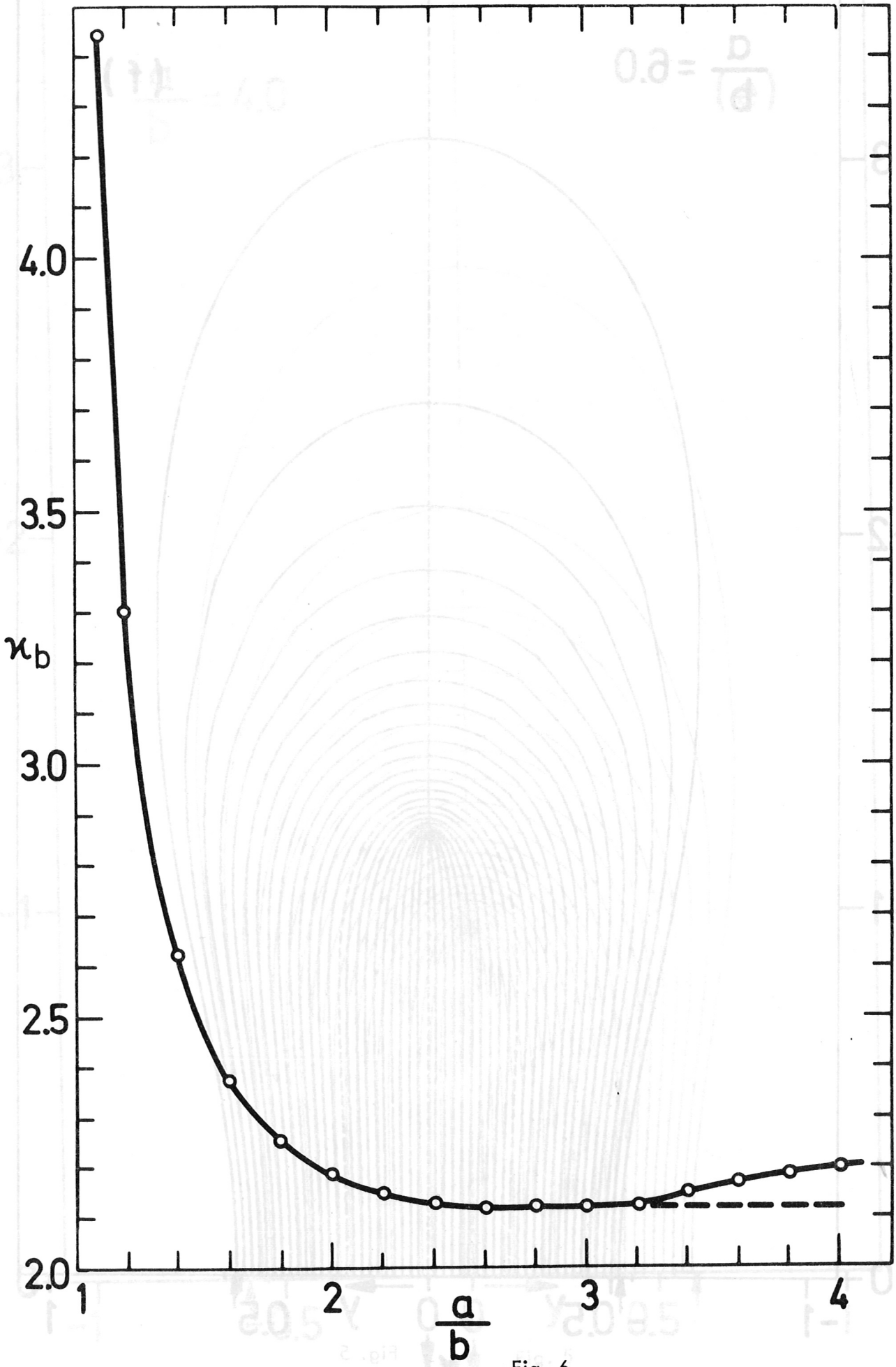

Fig. 6

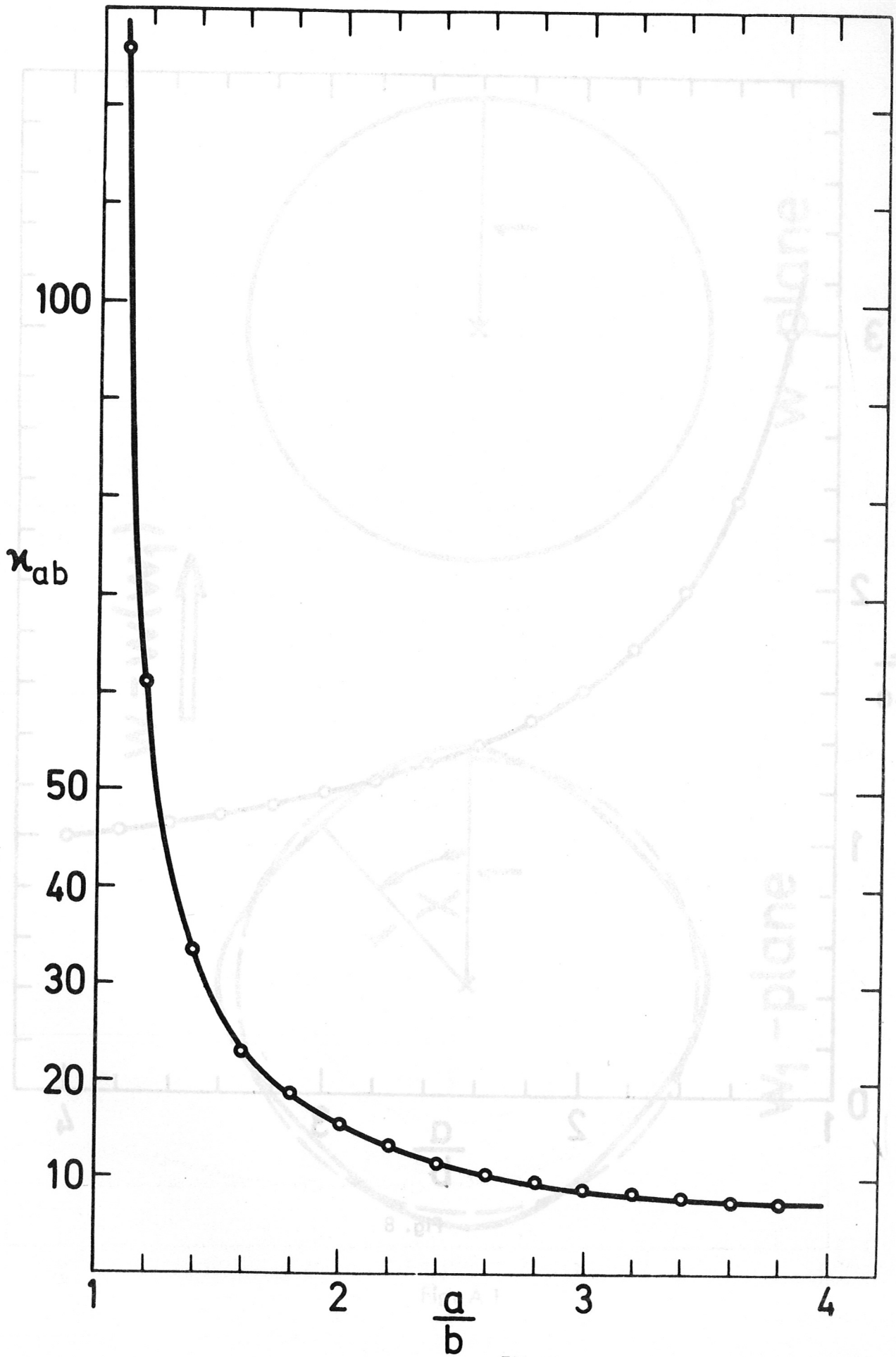

Fig. 7

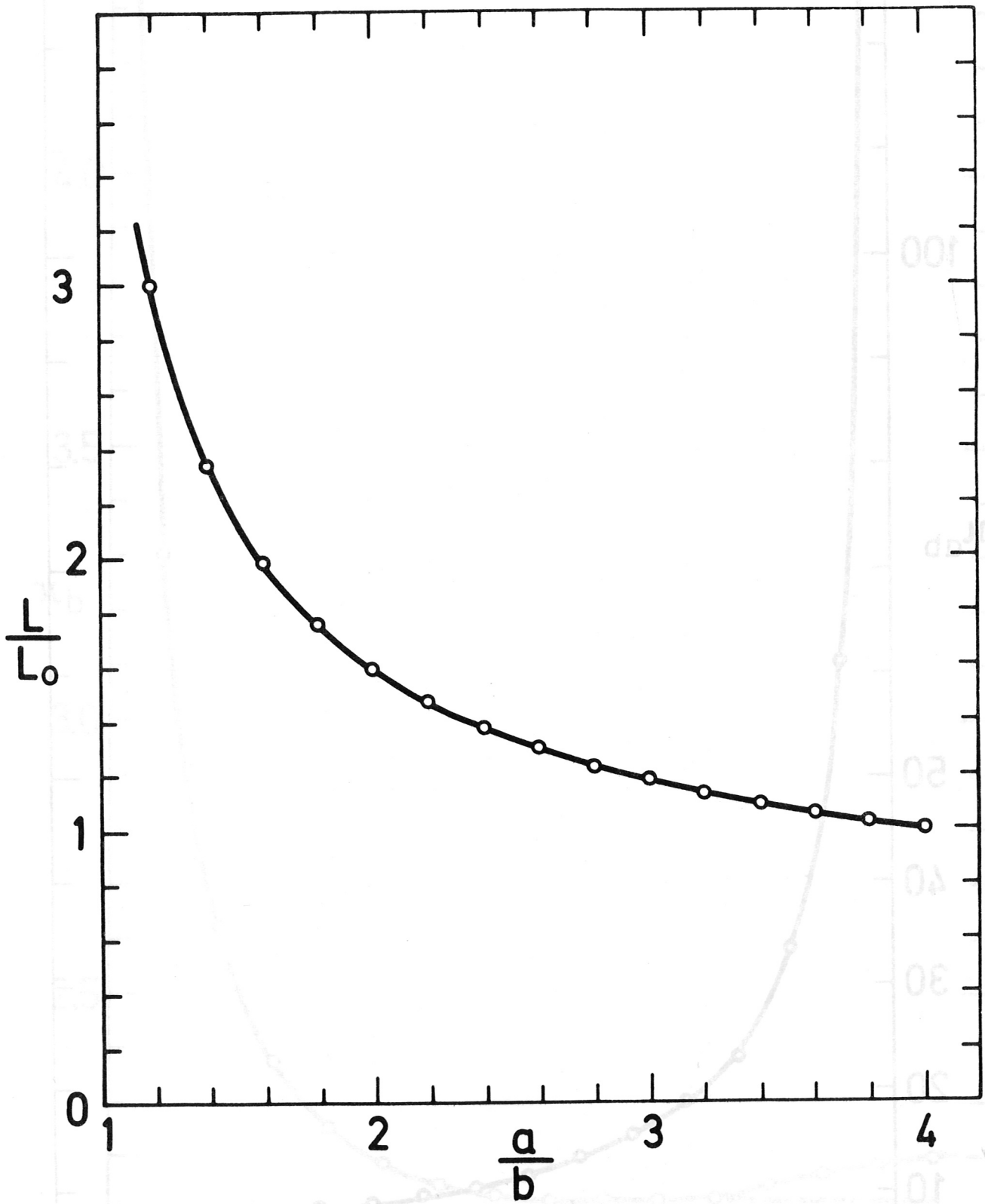

Fig. 8

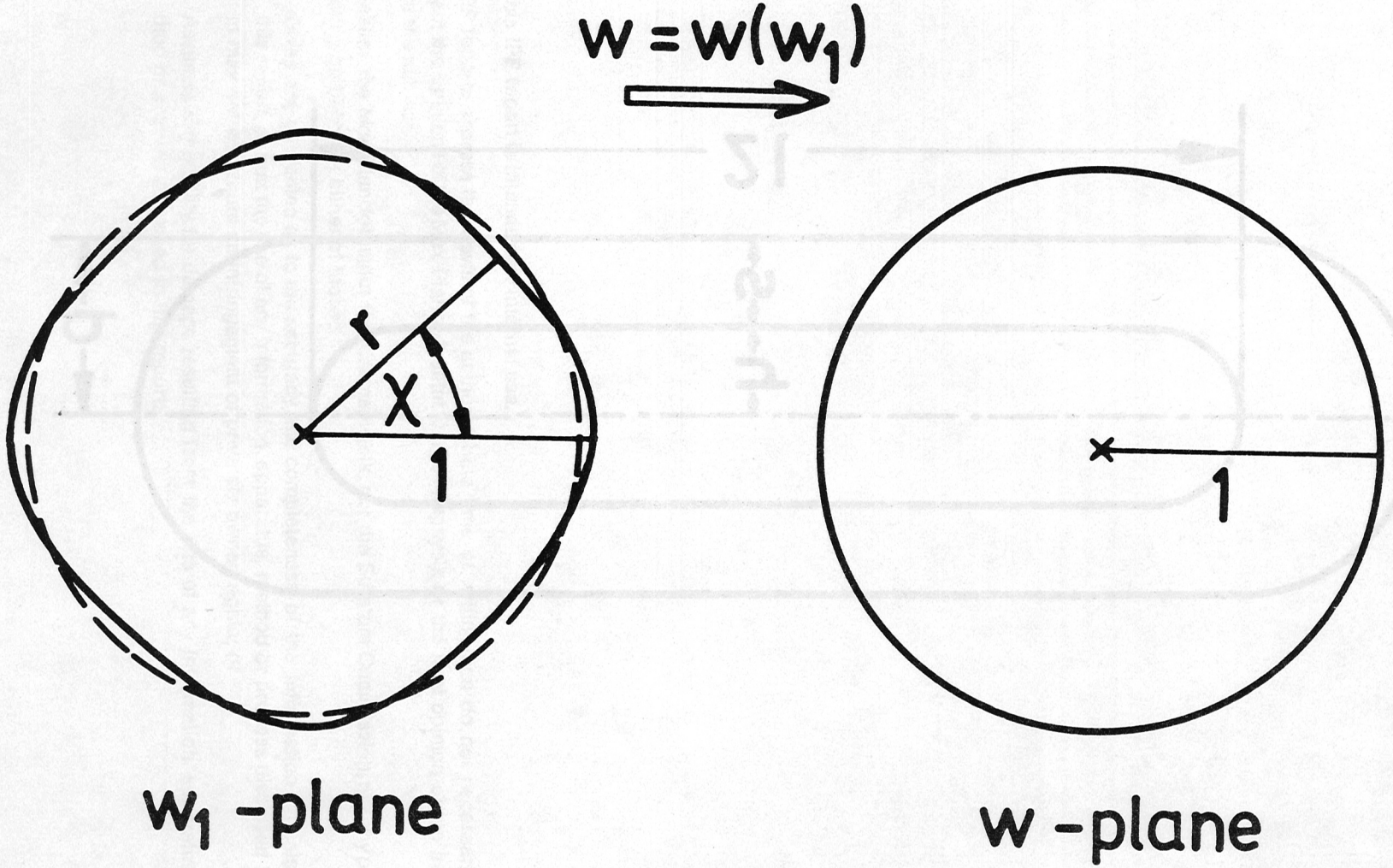

Fig. A 1

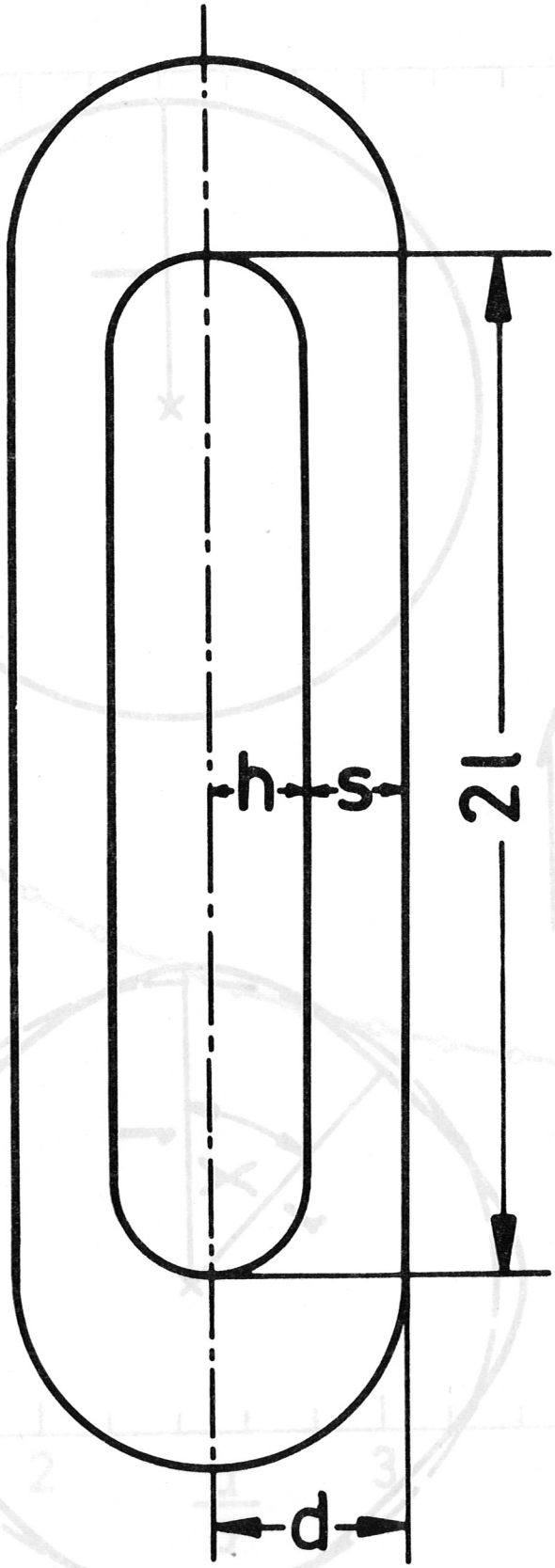

Fig. B 1